Quasi-isentropic compression using compressed water flow generated by underwater electrical explosion of a wire array

V. Gurovich,[1] A. Virozub,[1] A. Rososhek,[1] S. Bland,[2] R. B. Spielman,[3] and Ya. E. Krasik[1]
[1]*Physics Department, Technion, Haifa 32000, Israel*
[2]*Institute of Shock Physics, Imperial College London, London SW7 2BW, United Kingdom*
[3]*Department of Physics, Idaho State University, Pocatello, Idaho 83209, USA*

(Received 22 January 2018; accepted 24 April 2018; published online 9 May 2018)

A major experimental research area in material equation-of-state today involves the use of off-Hugoniot measurements rather than shock experiments that give only Hugoniot data. There is a wide range of applications using quasi-isentropic compression of matter including the direct measurement of the complete isentrope of materials in a single experiment and minimizing the heating of flyer plates for high-velocity shock measurements. We propose a novel approach to generating quasi-isentropic compression of matter. Using analytical modeling and hydrodynamic simulations, we show that a working fluid composed of compressed water, generated by an underwater electrical explosion of a planar wire array, might be used to efficiently drive the quasi-isentropic compression of a copper target to pressures $\sim 2 \times 10^{11}$ Pa without any complex target designs. *Published by AIP Publishing.*
https://doi.org/10.1063/1.5023165

I. INTRODUCTION

The study of matter at extreme conditions is a key issue in modern physics of warm dense matter due to the importance of this research for astrophysics,[1] planetary science,[2] and inertial confinement fusion.[3] The main subject of this research is the measurement of the equation-of-state (EOS) of matter and its related transport parameters, such as electrical and thermal conductivities, at extremely high pressures.

Several methods can be used to provide high pressures. The most common dynamic method is through shock compression, where a high-speed flyer accelerated by, for instance, a gas gun, impacts a target. However, this method can lead to a large entropy jump behind the shock wave (SW) in the target, resulting in a significant increase in temperature. For many applications, such as planetary physics, the temperatures obtained in shock physics experiments are far beyond those required, inducing unwanted phase changes in the material under study. In the last decade, much work, instead, concentrated on producing quasi-isentropic loading allowing one to achieve high compression without the associated huge increases in temperature. Several methods have been developed to achieve this, for instance, using a "graded density impactor" where a composite flyer consisting of several layers of the material with different acoustic impedances is accelerated using a light gas gun to hit the target; the ablative pressure of plasma produced at the surface of a target by temporally shaped laser beams is used,[4,5] temporally shaped magnetic pressure can be applied to conductors,[6] and ramp-wave compression can be generated by chemical explosives.[7,8]

Whether for shock or quasi-isentropic loading, most methods to produce high pressures are expensive, requiring large gas guns, pulsed-power accelerators, or large laser systems. Recently, an alternative method to drive strong SWs in water has been developed at Technion, where the electrical explosion of wires and wire arrays in water demonstrated the production of planar, cylindrical, and quasi-spherical shock waves in water.[9] The main advantages of this approach are related to the high efficiency (up to 24%) of the energy transfer from the exploding wire to the generated water flow and the relatively compact, low-cost, potentially long-rise-time (μs) pulsed-power generators employed.

In this paper, we present the first analytic and numerical calculations of how such a system of exploding wires in water could be used to quasi-isentropically load a copper target. In Sec. II, we compare compression of a copper target in the Hugoniot and isentropic approaches and determine a pressure where the Hugoniot and the isentrope diverge by only $\sim$10% in internal energy. In Sec. III, analytical modeling of a copper target compressed by a water shock wave is presented, and the parameters of the water flow and shock satisfying the conditions of the target isentropic compression are determined. In Sec. IV, the results of one-dimensional (1D) hydrodynamic (HD) modeling of the isentropic compression of a copper target by water flow are presented, and in Sec. V, we summarize the results obtained.

II. BACKGROUND: THE DIFFERENCE BETWEEN THE HUGONIOT AND THE ISENTROPE AT DIFFERENT SHOCK PRESSURES

The polytropic equation-of-state (EOS) is often in analytic studies of SW compression

$$P(\delta) - P_0 = A(S)[\delta^n - 1], \tag{1}$$

where n is the adiabatic index, P_0 is the pressure at normal conditions, $\delta = \rho/\rho_0$ is the compression ratio, and ρ and ρ_0 are the material densities in the case of compression and normal conditions, respectively. Parameter A, in the general case, depends on the entropy S of the material. In the case $A =$ Constant, one can consider an adiabatic process, which can be reversible or irreversible. In the case for copper (Cu),

the adiabatic index is $n=4$ and the constant is $A_{Cu} = 2.5 \times 10^{10}$Pa.[10]

For a SW, using the jump conditions and the polytropic EOS, the relationship between the specific internal energy (ε), pressure (P), and volume ($1/\rho$) behind the front of the SW can be written as

$$\begin{aligned}\varepsilon_s - \varepsilon_0 &= 0.5[P(\delta) + P_0](1/\rho_0 - 1/\rho) \\ &= 0.5\left[\frac{2P_0}{\rho_0} + \frac{A}{\rho_0}[\delta^n - 1]\right]\left(1 - \frac{1}{\delta}\right). \end{aligned} \quad (2)$$

In the case of an *isentropic* compression, we can instead obtain from the Fundamental Theorem of Thermodynamics

$$d\varepsilon = \left\{P_0 + A[\delta^n - 1]\right\}\frac{d\delta}{\rho_0\delta^2}. \quad (3)$$

Thus, in the case of the *isentropic* process, the increase in internal energy reads

$$\varepsilon_i - \varepsilon_0 = \frac{P_0}{\rho_0}\left(1 - \frac{1}{\delta}\right) + \left(\frac{A}{\rho_0}\right)\left[\frac{(\delta^{n-1} - 1)}{n-1} - \left(1 - \frac{1}{\delta}\right)\right]. \quad (4)$$

Here, let us note that for significant compression ($\delta \geq 1.1$), the term containing (P_0/ρ_0) on the right side of Eqs. (2) and (4) is significantly smaller and thus negligible compared to the term multiplied by (A/ρ_0). One can see similarity in the change of the internal energy in the case of a shock (i.e., compression on the Hugoniot) and the case of isentropic compressions of the material. The deviation of the isentropic compression from the adiabatic approximation can be estimated as

$$K(\delta) = \frac{\varepsilon_s - \varepsilon_0}{\varepsilon_i - \varepsilon_0}. \quad (5)$$

Let us define a deviation of $<10\%$ in internal energies as being "quasi-isentropic loading." In copper, this 10% deviation is given by a "critical" compression ratio of $\delta = \delta_{cr} \approx 1.12$, corresponding to critical pressure $P_c \approx P_{Cu} = 1.43 \times 10^{10}$ Pa. For SWs in the copper producing smaller jumps in pressure, one can consider that the Hugoniot closely follows the isentrope; for instance, both pressure and temperature vary approximately linearly with energy, and so, there are no large changes in the state variables. At higher compression ratios, the isentrope and the Hugoniot, both being adiabatic processes, significantly diverge. This effect is well known, hence the use of experiment when one replaces high pressure shock with multiple smaller shocks having the same peak pressure, but with lower heating of the shocked material. In the case of shock compression of water, a deviation from adiabatic processes of 10% corresponds to a compression ratio of $\delta_{cw} \approx 1.07$ and a pressure of only $P_{cw} \approx 1.87 \times 10^8$Pa, as water is much more compressible than copper.

III. COMPRESSION OF A COPPER TARGET BY A WATER SHOCK WAVE (ANALYTICAL MODELING)

As a first order approximation, let us consider the impact interaction of the SW generated in water with a Cu target. Considering the compression of copper to the same "critical" pressure as discussed in Sec. II, i.e., to a pressure where the Hugoniot and the isentrope diverge by only $\sim$10%, one can calculate the compression of the water at the water–copper boundary required to make this pressure using the polytropic EOS for water $P_w(\delta) - P_0 = A_w[\delta_w^n - 1]$, $n = 7.15$, $A_w = 3 \times 10^8$ (Pa). This gives a compression $\delta_w = 1.72$ which is far above the "critical" compression ratio of water. In reality, the compression of the target by the water flow requires the consideration of waves that are realized in the water, in the target, and at the water-target boundary. It is understood that, even with the application of the polytropic equations, an analytic solution of this problem becomes very challenging.

Nevertheless, let us consider a simplified case of the interaction of water flow having velocity V_{Iw} with a Cu target without taking into account the dynamics of the piston generating this flow and the shock wave multi-reflections (see Fig. 1). If, behind the front of the shock wave propagating in the target, the pressure is P_c, then the velocity of the SW front with respect to the Cu target (laboratory frame of reference) is

$$D = \sqrt{\frac{(P_c - P_0)\delta_c}{\rho_0(\delta_c - 1)}}, \quad (6)$$

where $\rho_0 \approx 9 \times 10^3$ kg/m^3 is the copper specific density at normal pressure P_0. For $\delta_c = \delta_{cr} = 1.12$ and $P_c \approx 1.43 \times 10^{10}$ Pa, the SW front velocity reaches $D = 3.86 \times 10^3$ m/s. The copper mass velocity behind the SW front can be calculated as

$$V_{Cu} = \sqrt{\frac{(P_c - P_0)(\delta_c - 1)}{\delta_c\rho_0}} \approx 413 \text{ m/s}. \quad (7)$$

Let us note that the water flow at the boundary of the target propagates with the same velocity $V_W = V_{Cu}$ and direction as SW in the target. The front velocity of the SW reflected from the target has value D_2, and this SW propagates in the direction opposite to the direction of the water flow. At the front of this reflected SW, one can write the conservation law for the mass of the water flux $\rho_{1w}(V_{1w} + D_2) = \rho_{2w}(V_w + D_2)$, and using the conservation law of

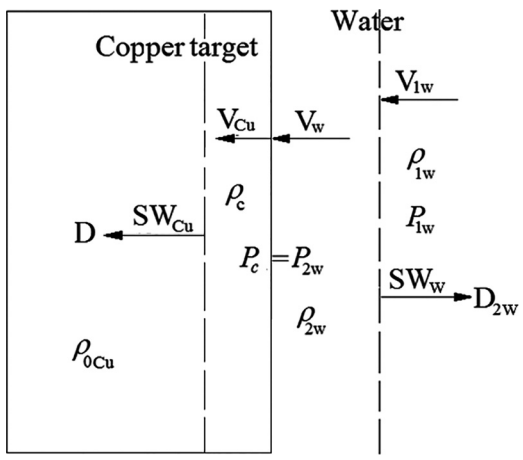

FIG. 1. Water flow interaction with a Cu target.

the flux of the momentum at the SW $P_{1w}+\rho_{1w}(V_{1w}+D_2)^2 = P_{2w}+\rho_{2w}(V_w+D_2)^2$, one obtains

$$V_{1w}+D_2 = \sqrt{\frac{P_{2w}-P_{1w}}{\rho_{1w}(1-\rho_{1w}/\rho_{2w})}};$$
$$V_w+D_2 = \sqrt{\frac{P_{2w}-P_{1w}}{\rho_{2w}(\rho_{2w}/\rho_{1w}-1)}}. \quad (8)$$

Now, excluding D_2 from these equations, we obtain

$$V_{1w}-V_w = \sqrt{\frac{(P_{2w}-P_{1w})}{\rho_{0w}}} \times \left[\sqrt{\frac{\delta_{2w}}{\delta_{1w}(\delta_{2w}-\delta_{1w})}}-\sqrt{\frac{\delta_{1w}}{\delta_{2w}(\delta_{2w}-\delta_{1w})}}\right]. \quad (9)$$

Here, the water compression ratios are $\delta_2 = \rho_{2w}/\rho_{0w}$ and $\delta_1 = \rho_{1w}/\rho_{0w}$, where ρ_{0w} is the water density at normal conditions. In this equation, we know the water compression at the water-target boundary $\delta_{2w} \approx 1.72$, the water flow $V_w = 413\,\mathrm{m/s}$, and the pressure in the water $P_{2w} = 1.43 \times 10^{10}\mathrm{Pa}$. Taking into account the EOS for water, Eq. (9) can be re-written as

$$(V_{1w}-V_w) = C_0\left[\sqrt{\frac{(\delta_{2w}^n-\delta_{1w}^n)\delta_{2w}}{n\delta_{1w}(\delta_{2w}-\delta_{1w})}}-\sqrt{\frac{(\delta_{2w}^n-\delta_{1w}^n)\delta_{1w}}{n\delta_{2w}(\delta_{2w}-\delta_{1w})}}\right]. \quad (10)$$

Here, $C_0 = \sqrt{A_w n/\rho_{0w}}$ is the speed of sound in water at normal conditions. In Eq. (10), there are two unknowns, namely, the velocity of the primary water flow V_{1w} and its compression ratio δ_{1w}. The value of V_{1w} can be determined using the compression factor δ_{1w} as

$$V_{1w} = C_0\sqrt{\frac{(\delta_{1w}^n-1)(1-1/\delta_{1w})}{n}}. \quad (11)$$

Substituting Eq. (11) in Eq. (10), one obtains required compression of the primary water flow $\delta_{1w} \approx 1.5$ for the known values $\delta_{2w} \approx 1.72$, $V_w = 413\,\mathrm{m/s}$, and $P_{2w} = 1.43 \times 10^{10}\,\mathrm{Pa}$. The ratio $\delta_{1w} \approx 1.5$ can be used to calculate the values of the primary water velocity $V_{1w} \approx 1.33 \times 10^5\mathrm{cm/s}$, the pressure behind the front of the primary SW $P_1 \approx 5.3 \times 10^9\mathrm{Pa}$, and the velocity of this primary SW $D_1 \approx 4 \times 10^5\mathrm{cm/s}$. These values of δ_{1w}, V_{1w}, P_1, and D_1 for the primary water flow and the SW interacting with the Cu target satisfy the conditions of isentropic compression of this target and can be achieved using an underwater electrical explosion of a planar wire array. For instance, in earlier experiments[11] with underwater electrical explosion of a planar wire array carried out using a microsecond-scale, high-current generator with a stored energy only of ~3.6 kJ and delivering a current with an amplitude of ~300 kA, the pressure and the expansion velocity of water flow reached ~10 MPa and ~5 × 10^5 cm/s, respectively.

IV. COMPRESSION OF A COPPER TARGET BY WATER FLOW (NUMERICAL MODELING)

The above considered analysis of the SW interaction with the target does not account for multi-reflections of the SW, which occur between the piston and the target. Indeed, the water compression wave, which interacts with the Cu target, is partially reflected and propagated towards the moving piston through the already compressed water layer. By reaching the piston, this wave experiences a reflection towards the Cu target and increases the pressure in the water layer by propagation towards the target. This multi-reflection process of the compression wave in the water layer with a moving piston is difficult to analyze analytically. Therefore, one dimension (1D) HD simulations were carried out to obtain the processes of the pressure evolution in the water layer and Cu target for different thicknesses of the water layer and target.

In this modeling, we consider the compression of a Cu target in a similar setup (see Fig. 1), but now the planar layer of water having thickness H_w is compressed by a moving piston propagating with velocity $V_p(t)$ that gradually increases in time. The latter can be realized by an electrical explosion of a wire array.[9,11] In fact, underwater electrical explosions of wires are accompanied by the generation of multiple, strong SWs, whose overlapping (in case of a planar wire array) leads to the formation of a single, planar SW propagating with a typical velocity of 3×10^5 cm/s in the vicinity of the exploding wire. In order to avoid the formation of a strong SW, the exploding wire radial expansion should be controlled by a corresponding tailored profile of the discharge current to prevent fast, liquid-vapor-plasma phase transitions. One can consider also electrical explosion of W, Ta, or Mo wire arrays. Preliminary research showed that the underwater electric explosion of a single W-wire drastically differs from the explosion of a Cu wire. The latter explosion is characterized by a critically damped discharge with a fast decrease in the discharge current amplitude during the wire explosion. An example of a shadow streak image of a single, W-wire underwater electrical explosion and the corresponding waveforms of the current and the resistive voltage with deposited power and energy is shown in Fig. 2. One can see that the W-wire explosion is characterized by an almost-constant discharge current during several hundreds of nanoseconds with the corresponding plateau in the deposited power and a rather gradual expansion of the exploding wire (details of this research will be presented elsewhere).

Thus, using either a temporally shaped current pulse or refractory wire materials, a gradual increase in the piston velocity can be realized, resulting in non-shocked water compression wave propagation to the water-Cu target boundary. When this water compression wave reaches the target, one obtains a compression wave propagating in the target with thickness H_{Cu}. When this compression wave in copper reaches the target right (free) boundary, the rarefaction wave is formed. This wave propagates to the left, and the target moves to the right. In the case of a known piston velocity $V_p(t)$, the time-dependent parameters of the compression wave in the Cu target plate depend on the thicknesses of the target and the water layer. The work produced by the piston during its motion is transferred to the potential energy of the water layer, and this potential energy is transferred to the target in the form of a compression wave. In order to achieve the largest amplitude in the compression wave in the target,

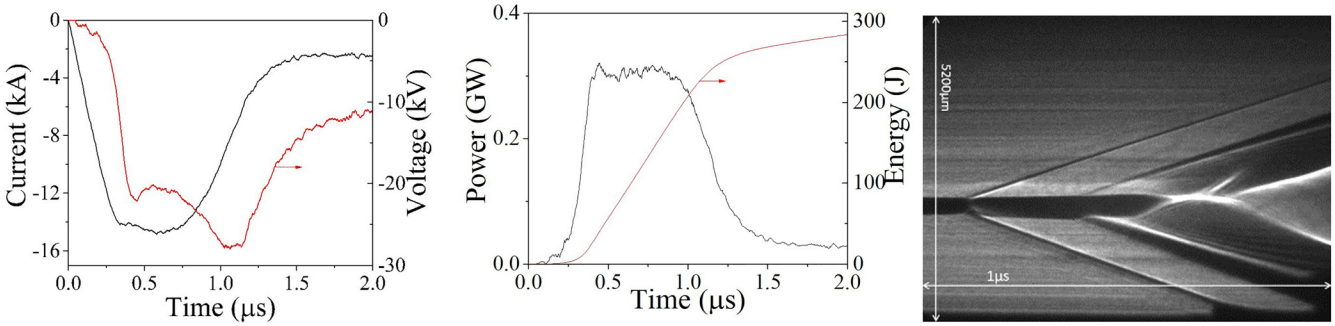

FIG. 2. A shadow streak image of a single W wire (0.2 mm in diameter and 40 mm in length) underwater electrical explosion and the corresponding waveforms of the current and resistive voltage with deposited power and energy.

one has to consider a relatively small thickness of the water layer H_W. Indeed, the energy density of compressed water determines the maximal pressure that can be achieved in the target. However, the parameters of the compression wave in the target depend also on its thickness H_{Cu}. Namely, in the case of the target s small thickness, the compression wave reaches the target free boundary earlier than one obtains the maximum pressure at the water-target boundary. From that time, the target starts to move, thus taking part of the energy of the compressed water layer.

In the present study, a planar piston–water–copper target system was modeled in a cylindrical domain with the copper/water boundary having an initial radius of 19 mm. The Cu target and water layer thicknesses were varied in the range of 1–3 mm. Depending on these parameters, the initial inner radius of the Cu target was varied in the range of 16–18 mm, while the initial outer radius of the piston was varied in the range of 20–22 mm. This cylindrical geometry is similar to that which one obtains in the case of a planar piston–target configuration due to the gap between the piston and the target being much smaller than its radii. The 1D HD simulations were based on the 1D piston model.[12,13] In this model, the outer boundary of the system is considered as a boundary of a cylindrical converging piston (rigid wall) pushing the adjacent water layer and generating a water flow. Euler's equations for an axially symmetric flow were used in the Lagrange form. The coordinate in these equations is the mass $m(r)$ enclosed in a cylindrical layer with density ρ for a given height at distance r from the axis. In addition to the original model described in Refs.12 and 13, the present simulations consider a two-domain system, namely, the water flow and the Cu target. Therefore, HD differential equations were coupled with the tabulated SESAME EOS[14] for water and copper. The boundary condition at the piston-water boundary determines the velocity of the piston, which was modeled as

$$V_p(t) = \begin{cases} V_m(t/t_r)^{2.5}, & t \le t_r \\ 0, & t > t_r \end{cases}, \tag{12}$$

where the maximal piston velocity $V_m = 3 \times 10^5$ cm/s is reached at $t = t_r = 2$ μs. The piston propagation is terminated when its velocity reaches the maximal value that can be achieved in experimental conditions.[8] The inner boundary of the Cu target is considered to be free, i.e., inside of the copper boundary is vacuum. The models include thermal transport. In the modeling, the increment of specific internal energy ε due to the thermal conductivity of matter $[\kappa(T)]$ is calculated as

$$d\varepsilon = -\frac{\partial(Qr^2)}{\partial m} dT, \tag{13}$$

where m is the mass variable, and the heat flux Q is

$$Q = -\kappa(T)\rho r^2 \frac{\partial T}{\partial m}. \tag{14}$$

The thermal conductivity is calculated as follows:[15] $\kappa_{Cu}(T) = 418,7775 - 0.07509T$ for $T < 1356$ K and $\kappa_{Cu}(T) = 89,7067 - 0.04976T$ for $3000\,\text{K} > T > 1356\,\text{K}$.

The 1D HD simulations were carried out for water layers of 1-mm, 2-mm, and 3-mm thicknesses. The Cu target thickness was also varied as 1 mm, 2 mm, and 3 mm for each value of the water layer thickness. The distributions of the pressure between the free boundary of the Cu target and the piston at 3 different times at and near the time of the maximal values of the pressure at the water/Cu target boundary are shown in Figs. 3–5. The maximal values of pressure at the water-target boundary, at the free target surface, and inside the target for different values of the water layer and target thicknesses are presented in Table I and Fig. 6.

First, one can see that even for a gradual increase in water flow pressure, one obtains formation of SW characterized by the pressure jumps at the front of the compression wave in the Cu target. The value of these pressure jumps can be as high as 3×10^{10} Pa, depending on the target and water-layer thicknesses. Nevertheless, the amplitude of this pressure jump does not exceed ~15% of the amplitude of the compression wave propagating in the Cu target. Let us note that the formation of these SW is related to the decreasing profile of the copper mass velocity and density space distribution towards the "free" boundary of the copper target. This leads to time-space bunching of the copper material, resulting in the formation of SWs inside the copper target propagating towards the "free" boundary. The results of simulations showed also that these pressure jumps are accompanied by only small inclines in density profiles. The results of simulations showed that, as expected, the compression of the target is accompanied by the heating process. For instance, the increase in the pressure from $\sim 3 \times 10^{10}$ Pa to $\sim 11 \times 10^{10}$ Pa leads to a gradual increase in the temperature from ~1000 K to 2500 K, respectively.

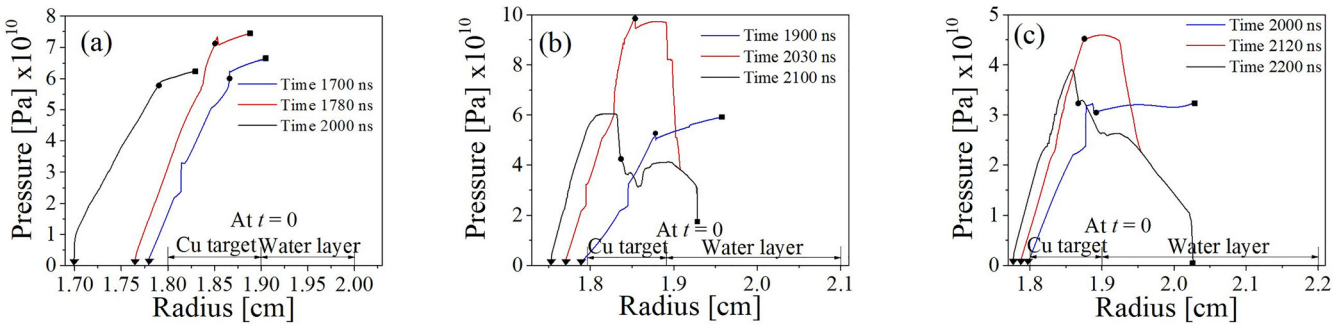

FIG. 3. Pressure distributions in a Cu target with thickness $H_{Cu} = 1$ mm and a water layer at different times of the target compression. Water layer thickness: (a) $H_w = 1$ mm ($t = 1.78$ μs corresponds to the maximal pressure at the target/water boundary), (b) $H_w = 2$ mm ($t = 2.03$ μs corresponds to the maximal pressure at the target/water boundary), and (c) $H_w = 3$ mm ($t = 2.12$ μs corresponds to the maximal pressure at the target/water boundary). Circles denote water/plate boundaries; squares denote the piston boundary; and triangles denote the free side of the target s boundary.

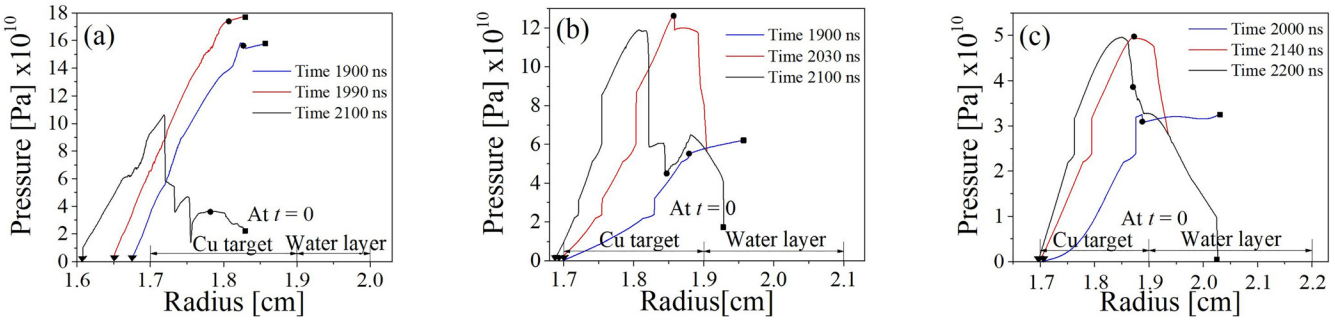

FIG. 4. Pressure distributions in a Cu target with $H_{Cu} = 2$ mm and a water layer at different times of the target compression. (a) Water layer $H_w = 1$ mm ($t = 1.99$ μs corresponds to the maximal pressure at the target/water boundary). (b) Water layer $H_w = 2$ mm ($t = 2.03$ μs corresponds to the maximal pressure at the target/water boundary). (c) Water layer $H_w = 3$ mm ($t = 2.14$ μs corresponds to the maximal pressure at the target/water boundary). Circles denote water/plate boundaries; squares denote the piston boundary; and triangles denote the free side of the target s boundary.

In the case of the Cu target with $H_{Cu} = 1$ mm, the maximal values of pressure at the water-target boundary and inside the target do not exceed $\sim 9.9 \times 10^{10}$ Pa, and this pressure is realized at $H_w = 2$ mm. This is because at $H_w = 1$ mm, the compression wave reaches the target free surface too early, leading to the energy transfer for the target motion, and at $H_w = 3$ mm, the energy density transferred to the water is smaller than for the case $H_w = 2$ mm.

In the case of the Cu target with $H_{Cu} = 2$ mm, the maximal values of the pressure at the water-target boundary and inside the target increase almost two times, up to $\sim 17.5 \times 10^{10}$ Pa, and this pressure is realized at $H_w = 1$ mm. This is because at $H_{Cu} = 2$ mm, significantly less energy is transferred to the target motion, and for $H_w = 2$ mm and $H_w = 3$ mm, the energy density transferred to the water is smaller than for the case $H_w = 1$ mm.

Finally, for the case of the Cu target with $H_{Cu} = 3$ mm and $H_w = 1$ mm, the maximal values of the pressure at the water-target boundary and inside the target increase further, reaching $\sim 2.1 \times 10^{11}$ Pa. At these conditions, one obtains the maximal energy density in compressed water and a negligibly small, energy transfer to the target motion. The distribution of the temperature and the density in the water and the Cu target for these conditions is shown in Fig. 7.

Thus, the obtained dependences of the pressure distribution showed that it is possible to obtain pressure values

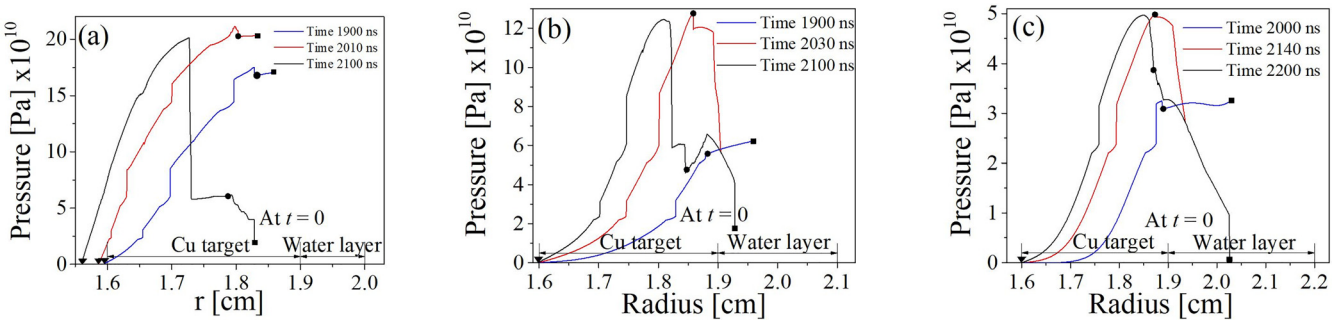

FIG. 5. Pressure distributions in a Cu target with $H_{Cu} = 3$ mm and a water layer at different times of the target compression. (a) A water layer $H_w = 1$ mm ($t = 2.01$ μs corresponds to the maximal pressure at the target/water boundary). (b) A water layer $H_w = 2$ mm ($t = 2.03$ μs corresponds to the maximal pressure at the target/water boundary). (c) A water layer $H_w = 3$ mm ($t = 2.14$ μs corresponds to the maximal pressure at the target/water boundary). Circles denote water/plate boundaries; squares denote the piston boundary; and triangles denote the free side of the target s boundary.

TABLE I. Maximal values of the pressure at the water target boundary, at the free target surface, and inside the target for different values of the water layer and target thicknesses.

Cu target thickness \ Water layer thickness		1 mm	2 mm	3 mm
1 mm	Maximal pressure at the water-target boundary/time	7.06×10^{10} Pa 1780 ns	9.91×10^{10} Pa 2030 ns	4.60×10^{10} Pa 2120 ns
	Maximal pressure at the free boundary of the target/time	1.49×10^{10} Pa 2500 ns	2.02×10^{10} Pa 2500 ns	0.78×10^{10} Pa 2500 ns
	Maximal pressure inside the target/time	7.04×10^{10} Pa 1780 ns	9.88×10^{10} Pa 2030 ns	4.58×10^{10} Pa 2120 ns
2 mm	Maximal pressure at the water/target boundary/time	17.5×10^{10} Pa 1990 ns	12.7×10^{10} Pa 2030 ns	5.01×10^{10} Pa 2140 ns
	Maximal pressure at the free boundary of the target/time	4.14×10^{10} Pa 2500 ns	1.45×10^{10} Pa 2500 ns	0.45×10^{10} Pa 2500 ns
	Maximal pressure inside the target/time	17.5×10^{10} Pa 1990 ns	12.7×10^{10} Pa 2030 ns	5.02×10^{10} Pa 2140 ns
3 mm	Maximal pressure at the water/target boundary/time	20.5×10^{10} Pa 2010 ns	12.8×10^{10} Pa 2030 ns	5.01×10^{10} Pa 2140 ns
	Maximal pressure at the free boundary of the target/time	1.49×10^{10} Pa 2460 ns	0.95×10^{10} Pa 2500 ns	1.03×10^{10} Pa 3000 ns
	Maximal pressure inside the target/time	21.2×10^{10} Pa 2010 ns	12.8×10^{10} Pa 2030 ns	5.02×10^{10} Pa 2140 ns

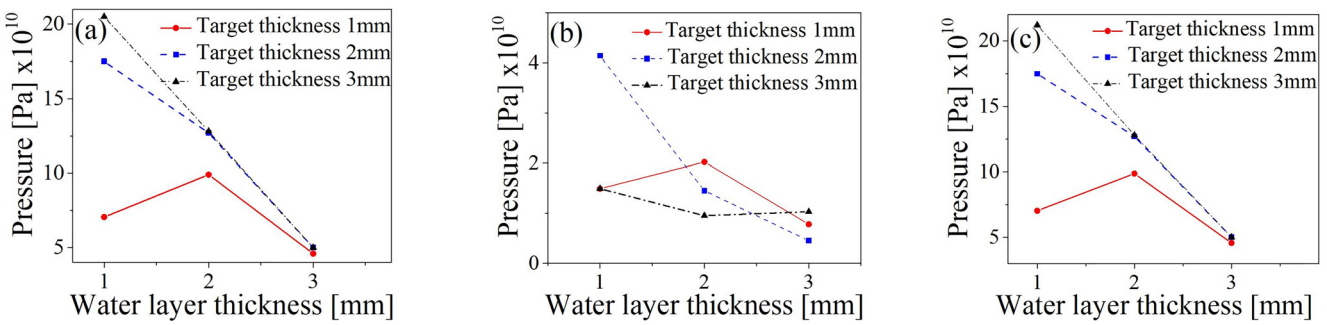

FIG. 6. Maximal (in time) values of the pressure at the water-target boundary (a), at the free target surface (b), and inside the target (c) versus water layer thickness for different values of the target thickness.

exceeding 2×10^{11} Pa in a Cu target using a compressed flow of water generated by the moving piston. This high value of pressure can be obtained without a liquid-vapor phase transition of copper, which requires a boiling temperature of 2835 K.

It is interesting to compare the parameters, which the copper acquires, when the pressure reaches 2×10^{11} Pa in the case of quasi-isentropic and shock compression. In order to make this comparison, additional simulations were carried out. In these simulations, we considered the compression

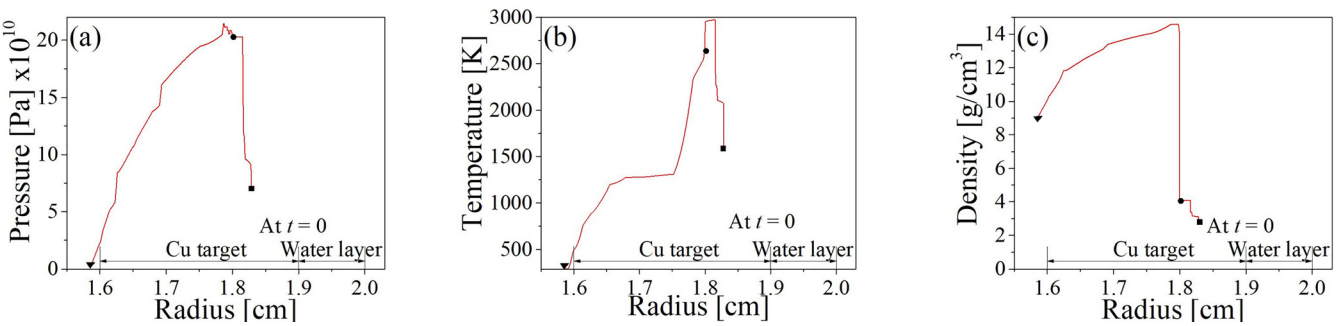

FIG. 7. Pressure (a), temperature (b), and density (c) distributions in a copper plate with a thickness of 3 mm and a water layer with a thickness of 1 mm at $t = 2010$ ns corresponding to the maximal pressure at the target/water boundary. Circles denote water/plate boundaries; squares denote the piston boundary; and triangles denote left side target s boundary.

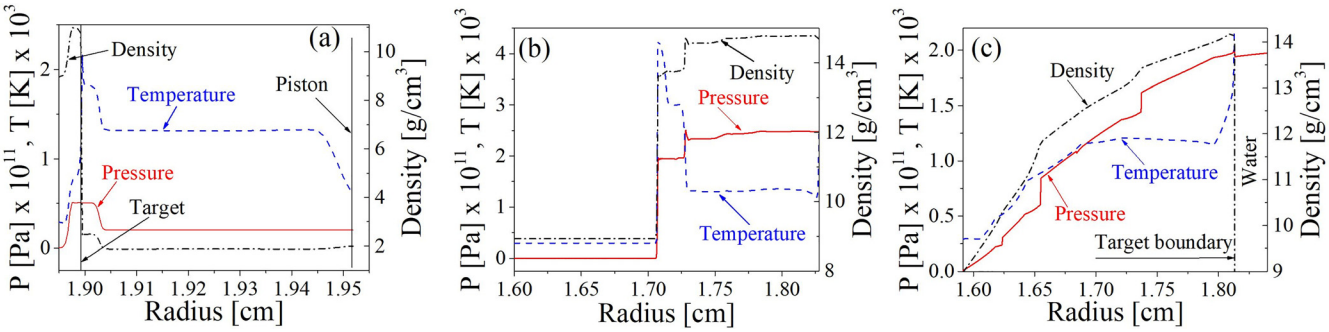

FIG. 8. Radial distributions of the pressure, temperature, and density: (a) in water between the piston and the Cu target (3-mm thick) at $t = 170$ ns when the shockwave in water has approached the target; (b) at $t = 500$ ns when the shockwave propagates inside the Cu target at the distance of ~1.25 mm with respect to the target-water boundary which is located at that time at the radius of ~1.83 cm; and (c) at $t = 1960$ ns for the case of quasi-isentropic compression. The time t is considered with respect to the beginning of the piston propagation.

wave propagating in a 1-mm-thick water layer and interacting with a 3-mm thick copper target. This compression wave can be generated by a planar wire array from which electrical explosion is modeled by a piston, whose fast expansion generates a compression wave in water. Initial radial positions of the piston and outer boundary of the copper target are at radii of 2 cm and 1.9 cm, respectively. In order to obtain a shockwave propagating in copper with a pressure of 2×10^{11} Pa behind its front, the piston velocity was modeled as $V_p = V_m(t/t_r)$, $t < t_r$ and $V_p = V_m$, $t \geq t_r$. Here, the piston maximal velocity $V_m = 3000$ m/s is reached at $t_r = 20$ ns. The radial distributions of pressure, temperature, and density for the case of shockwave and quasi-isentropic compression of the copper target are shown in Fig. 8.

In Fig. 8(a), one can see parameters of water flow at $t = 170$ ns relative to the beginning of the piston propagation. At this time, the shockwave propagating in water has approached the copper target and the compression wave propagates in the target for 10 ns at the distance of ~40 μm with respect to the target s boundary. The pressure at the target-water boundary increases up to 1.5×10^{11} Pa, and the temperature reaches ~2100 K. The parameters of copper, behind the front of the shockwave propagating in the target at $t = 500$ ns, i.e., at the distance of ~1.25 mm from the water-target boundary, are shown in Fig. 8(b). One can see that the values of pressure, temperature, and density behind the shockwave front experience jumps from their corresponding values at normal conditions to 2×10^{11} Pa, 4200 K, and 13.6 g/cm^3, respectively. For comparison, the parameters of copper in the case of quasi-isentropic compression at $t = 1960$ ns are shown in Fig. 8(c). This compression wave was generated in the same geometry as the one for shockwave compression, but the piston motion was modeled as $V_p = V_m(t/t_r)^{2.5}$, where $t_r = 2000$ ns. One can see that the pressure and density reach 2×10^{11} Pa and ~14 g/cm^3, respectively, at the target-water boundary, while the temperature does not exceed 2000 K which is 2.1 times smaller than in the case of shockwave compression.

V. CONCLUSIONS

We have carried out analytical modelling of the interaction of a strong shockwave, generated by underwater wire electrical explosion, with a copper target that indicated the possibility of a quasi-isentropic target compression. Numerical modelling, which took into account multiple wave reflections, demonstrated the need for a more gradual expansion of the wires, which if achieved could result in quasi-isentropic target compression up to 2×10^{11} Pa with a relatively small input of energy to the wires.

In the experiments, we use a planar array of 60 wires, each of ~100 μm in diameter and a length of ~30 mm with a distance between wires of ~0.25 mm. This wire array will be placed in a stainless-steel box at a distance of 1 mm from the upper cover, and the target will be placed beneath from the wire array, at variable (1 mm–3 mm) distances. In the case of a total discharge current with a maximal amplitude of ~500 kA, the current through each wire will be 8.3 kA and the current density will reach 10^8 A/cm^2. A planar SW, formed by the overlapping of the SWs generated by each wire explosion, will be formed at a typical distance of ~0.25 mm with respect to the wire array. The main technical challenge in this research will be obtaining a gradual expansion of the wire array without a sharp electrical explosion, which can be achieved by using wires made of refractory metals. Earlier experimental and numerical studies of tungsten wire underwater electrical explosion in microsecond[16,17] and nanosecond[18] timescales showed different temporal behaviors of the conductivity than those found in the case of explosion of aluminum[18] or copper[19] wires. This difference is related to different rates of melting and evaporation, resulting in a rather long duration plateau of the discharge current. The latter could allow one to obtain gradual radial expansion of the wire without generation of strong shockwaves.

[1]B. A. Remington, R. P. Drake, and D. D. Ryutov, Rev. Mod. Phys. **78**, 755 (2006).
[2]G. Huser, M. Koening, A. Benuzzi-Mounaix, T. Vinci, B. Faral, M. Tomossini, B. Telaro, and D. Batani, Phys. Plasmas **12**, 060701 (2005).
[3]M. D. Knudson, D. L. Hanson, J. E. Bailey, C. A. Hall, J. R. Asay, and W. W. Anderson, Phys. Rev. Lett. **87**, 225501 (2001).
[4]D. C. Swift and R. P. Johnson, Phys. Rev. E **71**, 066401 (2005).
[5]N. Amadou, E. Brambrink, A. Benuzzi-Mounaix, T. Vinci, T. de Rességuier, S. Mazevet, G. Morard, F. Guyot, N. Ozaki, K. Miyanishi, and M. Koenig, "Laser-driven quasi-isentropic compression experiments and numerical studies of the iron Alpha-epsilon transitions in the context of planetology," AIP Conf. Proc. **1426**, 1525–1528 (2012).
[6]J.-P. Davis, C. Deeney, M. D. Knudson, R. W. Lemke, T. D. Pointon, and D. E. Bliss, Phys. Plasmas **12**, 056310 (2005).

[7]J. F. Barnes, P. J. Blewett, R. G. McQueen, K. A. Meyer, and D. Venable, J. Appl. Phys. **45**, 727 (1974).
[8]M. A. Mochalov, R. I. Il kaev, V. E. Fortov, A. L. Mikhailov, A. O. Blikov, V. A. Ogorodnikov, V. K. Gryaznov, and I. L. Iosilevskii, J. Exp. Theor. Phys. **124**, 505 (2017).
[9]Y. E. Krasik, S. Efimov, D. Sheftman, A. Fedotov-Gefen, O. Antonov, D. Shafer, D. Yanuka, M. Nitishinskiy, M. Kozlov, L. Gilburd, G. Toker, S. Gleizer, E. Zvulun, V. T. Gurovich, D. Varentsov, and M. Rodionova, IEEE Trans. Plasma Sci. **44**, 412 (2016), and references therein.
[10]Y. B. Zeldovich and Y. P. Raizer, in *Physics of Shock Waves and High-Temperature Hydrodynamic Phenomena*, edited by W. D. Hayes and R. R. Probstein (Dover Publications Inc., 2002).
[11]S. Efimov, V. T. Gurovich, G. Bazalitski, A. Fedotov, and Y. E. Krasik, J. Appl. Phys. **106**, 073308 (2009).
[12]A. Grinenko, V. T. Gurovich, and Y. E. Krasik, Phys. Plasmas **14**, 012701 (2007).
[13]G. Bazalitski, V. T. Gurovich, A. Fedotov-Gefen, S. Efimov, and Y. E. Krasik, Int. J. Shock Waves, Detonations Explos. **21**, 321 (2011).
[14]*Sesame: The Los Alamos National Laboratory Equation-of-State Database*, Los Alamos National Laboratory Report LA-UR-92-3407, edited by S. P. Lyon and J. D. Johnson, 1992.
[15]C. Cagran, "Thermal conductivity and thermal diffusivity of liquid copper," Ph.D. thesis (Institut fur Experimental Physik, 2000), and references therein.
[16]N. I. Kuskova, S. I. Tkachenko, and S. V. Koval, J. Phys.: Condens. Matter **9**, 6175 (1997).
[17]K. V. Khishchenko, S. I. Tkachenko, P. R. Levashov, I. V. Lomonosov, and V. Vorob ev, Int. J. Thermophys. **23**, 1359 (2002).
[18]V. I. Oreshkin, R. B. Baksht, A. Y. Labetsky, A. G. Rousskikh, A. V. Shishlov, P. R. Levashov, K. V. Khishchenko, and I. V. Glazyrin, Tech. Phys. **49**, 843 (2004).
[19]S. I. Tkachenko and N. I. Kuskova, J. Phys.: Condens. Matter **11**, 2223 (1999).